Temperature-induced martensitic phase transitions in gum-metal approximants: First-principles investigations for Ti_3Nb

Petr Lazar, Michal Jahnátek, and Jürgen Hafner*
Faculty of Physics and Center for Computational Materials Science, University of Vienna, Sensengasse 8/12, A-1090 Wien, Austria

Naoyuki Nagasako and Ryoji Asahi
Toyota Central Research and Development Laboratories, Incorporated, Nagakute, Aichi 480-1192, Japan

Claudia Blaas-Schenner, Markus Stöhr, and Raimund Podloucky
Institute for Physical Chemistry and Center for Computational Materials Science, University of Vienna, Sensengasse 8/7, A-1090 Wien, Austria

(Received 27 April 2011; published 2 August 2011)

We present a first-principles investigation of the structures and the dynamical stability of the austenite and martensite phases of binary Ti_3Nb alloys, used as a model system for the superelastic and superplastic gum-metal alloy. For the body-centered cubic high-temperature β phase, structural models are constructed by optimizing the chemical decoration of a large supercell and by a cluster expansion method. The energetically most favorable structure is found to be elastically stable but dynamically unstable in the harmonic approximation. At finite temperature anharmonic phonon-phonon interactions treated in a self-consistent phonon approximation stabilize the structure already at room temperature. For the low-temperature α', ω, and α'' phases stable structure models have been constructed. For the hexagonal α' phase a model is generated by optimizing the chemical decoration of a supercell based on the hexagonal B_h lattice. The hexagonal ω structure may be derived from the body-centered cubic β phase using the (111) plane collapse model. The structure of the orthorhombic α'' phase may be viewed as produced by a strain-induced transformation of the body-centered cubic β phase, albeit with a different chemical decoration. The relaxed structures of the α', ω, and α'' phases were found to be both elastically and dynamically stable in the low-temperature limit. The martensitic temperatures for the $\beta \rightarrow \alpha''$, $\beta \rightarrow \omega$, and $\beta \rightarrow \alpha'$ transitions were estimated by comparing the Helmholtz free energies as a function of temperature.

DOI: 10.1103/PhysRevB.84.054202 PACS number(s): 61.50.Ah, 61.50.Ks, 62.20.−x, 63.20.−e

I. INTRODUCTION

The phase stability of Ti alloys can be changed by adding alloying elements such as vanadium, niobium, molybdenum, or iron, most of which are known to stabilize the bcc β phase at ambient or elevated temperatures. The limit of bcc stability was shown to be determined by the vanishing of the shear modulus $C' = \frac{1}{2}(C_{11} - C_{12})$ and correlated to a critical electron-per-atom ratio of $e/a \sim 4.15$.[1,2] The stabilization of the β phase is of practical importance because it enhances deformation capability and strength of the alloy. Three kinds of phase transitions ($\beta \rightarrow \alpha', \alpha'', \omega$) have been reported for Ti-rich alloys.[2,3] The structure of α' martensite is closely related to the hexagonal low-temperature α phase of pure Ti, the formation of which is limited to low concentrations of the alloying element. Above a critical alloying content a martensitic transformation to the orthorhombic α'' phase is observed. The reversible $\beta \leftrightarrow \alpha''$ transition results in a shape-memory effect.[4] The ω phase can be formed as a metastable phase, at low solute content by quenching from the β phase, at higher solute content by isothermal aging close to the martensite temperature.[5] The structure of the ω phase is either hexagonal or trigonal. Moffat and Larbalestier[3] have investigated the competition between the formation of α'' and ω phases in Ti-Nb alloys upon quenching and aging. Fast quenching of alloys with 20–25 at. % Nb favors the formation of the α'' phase, while under slow quenching conditions the ω phase is formed. Aging of air-cooled samples at temperatures above 400°C leads to formation of α'' precipitates, while aging at temperatures below 400°C favors formation of the ω phase. The formation of α'' and ω precipitates was found to be mutually exclusive; no transformations between both low-temperature phases was observed. A $\beta \rightarrow \alpha''$ transformation can also be induced by applying uniaxial strain. The plastic deformation of β-phase alloys is a complex process, because besides simple dislocation-motion deformation, twinning and stress-induced martensitic transformations play an important role. The dominant mechanism depends on alloy composition and/or the fabrication process.[6]

During the last decades, binary Ti-V,[7] Ti-Nb,[8–12] Ti-Ta,[13] and Ti-Mo[14] based alloys have been the focus of intense research efforts because their superelastic and shape-memory properties makes them suitable for many high-tech applications and detailed investigations of their martensitic transformations have been reported.[10] β-phase Ti alloys with Nb, Ta, and Zr have also been considered for biocompatible implants because they feature not only high strength, corrosion resistance, and nontoxicity, but also a low Young's modulus compatible with that of human bones.[15]

Detailed results for the martensitic transformations in binary Ti-Nb alloys with 15–35 at. % Nb have been reported by Kim *et al.*[10] The critical strain for the $\beta \rightarrow \alpha''$ transformation is found to decrease linearly with increasing Nb content. At a composition of Ti_3Nb the maximum transformation strain of 4.1% is reported for the [110] direction, and lower values

of 2.1% and 1.5% have been found for the [100] and [111] directions, respectively. The martensitic start temperature decreases from about 500 K at 20 at. % Nb to about 150 K at 30 at. % Nb, reaching room temperature at the composition Ti_3Nb. The critical stress for slip increases due to the fine subgrain structure of the ω precipitates, leading to stable superelasticity.

The name of gum-metal has been given to a class of Ti-Nb-Zr-O alloys which display high strength, a low elastic modulus, high yield strain, and a very good ductility developed at the Toyota Central Research and Development Laboratories.[16] These properties are achieved by adjusting the alloy composition such that the average electron-per-atom ratio comes close to a critical value of $e/a \sim 4.24$, for which *ab initio* calculations of the elastic constants of binary Ti-based alloys have predicted a vanishing tetragonal shear constant.[17] Under tensile loading the alloy deforms elastically until the stress approaches the value of the ideal strength of $\sigma \sim 1.5$ GPa estimated from the calculated elastic constants.[18–20]

It has been reported[21] that in gum-metal the large elastic deformation reaching 2.5% is not accompanied by martensitic phase transformation. Nanoindentation experiments reveal an unusual deformation pattern around the imprint of the nanoindenter[22] but no evidence for dislocation, twin, or fault propagation. In contrast, tensile and compressive loading of single-crystal specimens of gum-metal[23,24] and the compression of nanopillars of the material[25] studied *in situ* using transmission electron microscopy demonstrated that a deformation-induced transformation to the orthorhombic α'' phase takes place. Largely reversible stress-induced phase transformations during tensile loading and unloading were observed also using *in situ* synchrotron x-ray diffraction.[26,27] Formation of the α'' phase under stress was found to be very sensitive to the direction of the applied load. Single crystals oriented along (110) underwent a $\beta \rightarrow \alpha''$ transformation under tensile load, while crystals loaded along (111) or (100) did not transform at all. Compressive stress along (100) induces a martensitic transformation.

In contrast to the extensive experimental investigations of gum-metal and related alloys, only a very few attempts have been made to achieve a fundamental understanding of their outstanding properties by atomistic simulations. Saito *et al.*[16] suggested that the unique properties result from a dislocation-free plastic deformation mechanism called giant planar faults, which induces crystallographic rotations from the neighboring area by plastic deformation. Sun *et al.*[28] have calculated the total energies and elastic properties of the β, α'', and ω phases of Ti_3Nb using density-functional theory. Phase stability was found to decrease in the sequence $\alpha'' \rightarrow \omega \rightarrow \beta$ (assuming $D0_3$-type ordering in the β phase). The bulk moduli of all three phases were found to be of similar magnitude, but the shear and Young's moduli are lower in the β than in the α'' and ω phases. Li *et al.*[29] performed calculations of the elastic properties and the ideal tensile and shear strengths of bcc Ti-V alloys in a virtual crystal approximation. They demonstrated that at a critical composition of 75 at. % of Ti the alloy indeed shows exceptionally low values of the ideal tensile and shear strengths and proposed that a dislocation-free deformation takes place because the triggering stress for dislocation motion exceeds the ideal strength. However, details of the alloy structure and the relative stabilities of the competing martensitic phases of the alloy have not been investigated so far.

That the bcc high-temperature phases of many metals are stabilized by their large vibrational entropies was proposed long ago by Zener.[30] For the light alkali metals Li and Na and for LiMg alloys this conjecture has indeed been confirmed by quantitative calculations of the vibrational free energies, leading to reasonably accurate predictions of the martensitic temperatures.[31] Moroni *et al.*[32] have pointed out that for the stabilization of the bcc phases of the group IV transition metals Ti and Zr, both the vibrational and electronic entropies play an important role. However, in contrast to the bcc alkali metals and their alloys which are found to be dynamically stable in a harmonic approximation, the phonon spectra of bcc Ti and Zr calculated in a harmonic approximation reveal imaginary phonon frequencies at some wave vectors. Souvatzis *et al.*[33] have demonstrated that for Ti, Zr, and Hf the unstable phonon modes are stabilized at finite temperature by anharmonic phonon-phonon interactions treated in a self-consistent phonon approximation.[34–37] Very recently[38] this approach has been extended to the investigation of the stability of the bcc (B2-type) β phase of NiTi shape-memory alloys and of the premartensitic transition to a rhombohedral R phase (space group $P\bar{3}$). The investigations did not include the low-temperature martensitic phase, which is generally believed to crystallize in the monoclinic B19′ structure (space group $P2_1/m$).[39–41] Recent *ab initio* calculations have raised doubts about the structure of the martensitic phase of NiTi, suggesting that the experimentally reported B19′ phase might be stabilized by internal stress and that a B33 phase (space group $Cmcm$) has a lower energy.[42–44] Detailed studies of the deformation mechanisms under strain have demonstrated that although the B33 is lower in energy, its formation in bulk samples might be suppressed because the B2-to-B33 transformation requires an unusually large extension of one of the lattice constants. Thus, while for the NiTi alloys atomistic models for the structure of the austenitic and martensitic phases are available, our knowledge of the crystal structures of gum-metal and related alloys is far less complete.

The aim of the present work is to investigate the martensitic phase transitions in gum-metal approximants using *ab initio* calculations. Originally the intention was to extend the work of Ikehata *et al.*[17] on the elastic properties of binary gum-metal approximants with the $D0_3$ structure to a calculation of their phonon dispersion relations and vibrational free energies and to compare these results with similar calculations for the hexagonal and orthorhombic phases. However, difficulties already arose at a lower level. New calculations of the elastic constants of $D0_3$-type Ti-(V, Nb, Ta) alloys with improved all-electron methods found bcc Ti_3V and Ti_3Nb to be elastically unstable (negative values of C_{44}), and calculations of the formation energies for point defects also produced negative values for antisite defects in $D0_3$-type Ti_3Nb if a full relaxation in a large supercell was permitted. Hence the assumption that an ordered $D0_3$ structure provides a realistic model for the structure of the alloy turned out to be invalid, confronting us with the necessity to construct a better structural model. The search for a better description of the structure and the

investigation of the dynamical properties of the body-centered cubic, hexagonal, and orthorhombic phases are described below. While for the hexagonal and orthorhombic phases the optimized structures were found to be both elastically and dynamically stable, even the energetically most favorable bcc structure was found to be dynamically unstable, although elastically stable. Hence, the situation is similar to that of pure Ti, where the high-temperature bcc phase is dynamically unstable at low temperatures. Self-consistent phonon calculations have been used to demonstrate that at finite temperature the bcc phase is stabilized by anharmonic phonon-phonon interactions and to estimate the transition temperatures to the hexagonal and orthorhombic low-temperature phases.

II. COMPUTATIONAL METHODS

Our *ab initio* total-energy and force calculations are based on density-functional theory (DFT) as implemented in the Vienna *ab initio* simulation package (VASP).[45,46] A gradient-corrected functional has been used to describe electronic exchange and correlations.[47] Electron-ion interactions are treated within the projector-augmented-wave (PAW) method.[48,49] The plane-wave basis set contained components with kinetic energies up to 350 eV. The total energy was calculated with high precision, converged to 10^{-8} eV/atom. Forces acting on the atoms were calculated using the Hellmann-Feynman theorem,[50] and stresses on the unit cell were calculated using the generalized force theorem of Nielsen and Martin.[51] Structural relaxation was performed using a quasi-Newton algorithm or the GADGET routine developed by Bučko *et al.*[52] using generalized coordinates. The structural relaxation was stopped when all forces acting on the atoms, calculated according to the Hellmann-Feynman theorem, were converged to 10^{-3} eV/Å, and all components of the stress tensor except that conjugate to the imposed strain where converged to 0.05 GPa.

Structural models for the bcc β and hexagonal α' phases have been constructed by optimizing the chemical decoration of the sites in large supercells and subsequent structural relaxation. In addition, for the β phase cluster-expansion calculations[53] have been performed. Models for the orthorhombic α'' and hexagonal ω phases have been constructed by applying appropriate deformations to the bcc lattice for the β phase with different chemical decorations and subsequent relaxation. For calculation of the elastic constants we used the symmetry-general least-squares extraction method proposed by Le Page and Saxe[54] in connection with VASP. The cubic cells were submitted to $\pm\varepsilon_1$ and $\pm\varepsilon_4$ strains, the tetragonal cells were submitted additionally to $\pm\varepsilon_3$ and $\pm\varepsilon_6$ strains, and for the orthorhombic cells two more strains, $\pm\varepsilon_2$ and $\pm\varepsilon_5$, were added. For each set of strains $\pm\varepsilon_i$, three different magnitudes of 0.25%, 0.5%, and 0.75% were used. Atomic coordinates were relaxed at constant strains using the external optimizer developed by Bučko *et al.*[52] For calculation of the elastic constants the total energy was calculated with even higher accuracy, converged to 10^{-9} eV/atom.

Very fine k-point meshes are required to calculate the elastic shear constants (details are given below together with the information on the supercells used for the simulations). All integration meshes were constructed according to the Monkhorst-Pack scheme.[55] The integration over the Brillouin zone used the tetrahedron method with Blöchl corrections.[56]

For calculations of the vibrational frequencies of a system we utilized generalized density-functional perturbation theory as implemented in VASP.[57] The calculations were performed for supercells containing up to 32 atoms. Tests performed with a larger supercell containing 108 atoms showed that the phonon frequencies differ only little and the free energy is converged with respect to supercell size. The *PHONOPY*[58] package was used to visualize calculated phonon dispersions. The vibrational contribution to the free energy $F_{\mathrm{vib}}(V,T)$ is calculated using the phonon density of states $g(\omega)$ from the self-consistent phonon calculations as

$$F_{\mathrm{vib}}(V,T) = \int_0^\infty g(\omega)\left[\frac{\hbar\omega}{2} + k_B T \ln(1 - e^{-\hbar\omega/k_B T})\right] d\omega. \tag{1}$$

It has been demonstrated by Cochran and Cowley[37] that this gives a value of the entropy which is correct to leading order in the anharmonicity.

The electronic contribution to the free energy $F_{el}(V,T)$ is evaluated directly in VASP by using the Fermi-Dirac function for the smearing of the eigenvalues. The electronic contribution is obtained by using a smearing width σ appropriate for the temperature ($\sigma = k_B T$) and calculating the total energy difference with respect to $\sigma = 0$. The Helmholtz free energy was then calculated by

$$F(V,T) = E(V) + F_{el}(V,T) + F_{\mathrm{vib}}(V,T), \tag{2}$$

where $E(V)$ is the static lattice energy. Note that thermal expansion has been neglected, because it would make the calculations very time-demanding.

The bcc β phase was found to be dynamically unstable at low temperatures; it is stabilized only at finite temperatures by anharmonic interactions. Anharmonicity was included by means of the self-consistent ab initio lattice dynamical method (SCAILD) developed by Souvatzis *et al.*[33] The SCAILD method combines Born's self-consistent phonon approach[34–37] with accurate *ab initio* calculations of interatomic forces in a supercell. All phonons with wave vectors commensurate with the supercell are excited together in the same cell. Due to the simultaneous presence of all commensurate phonons, the interaction between different lattice vibrations is taken into account. The phonon frequencies are calculated in a self-consistent manner by alternating between DFT calculations of the Hellmann-Feynman forces acting on atoms displaced from their equilibrium positions, and calculations of improved phonon frequencies and atomic displacement vectors. The self-consistent loop represents a much larger computational effort compared to usual phonon calculations, because the forces have to be recalculated at each iteration. In our calculations, about 100 iterations were necessary to obtain converged phonon frequencies. Note that in the present calculations thermal expansion and phonon damping have been neglected, and all calculations were performed at constant volume using the calculated lattice constants. A more detailed description of the SCAILD method can be found in the Appendix.

III. STRUCTURAL MODELS FOR THE β, α', α'', AND ω PHASES OF Ti_3Nb ALLOYS

In all four structural variants, Ti-Nb alloys are generally characterized as disordered and a random distribution of the chemical species over the sites of the bcc, hexagonal, or orthorhombic lattices is assumed. Elementary excitations in disordered alloys can be described, in principle, by two different approaches: (i) The structure of the alloys can be approximated by a large supercell whose sites are occupied such as to minimize the total energy of the system. Electronic or vibrational spectra can be calculated via diagonalization of the Hamiltonian or dynamical matrices. (ii) The disordered alloy is described by an effective periodic Hamiltonian constructed at different levels of theory—the virtual crystal approximation (VCA), the average T-matrix approximation (ATA), or the coherent potential approximation (CPA).[59–61] For a comparative discussion of the effective Hamiltonian and supercell approaches applied to harmonic phonons in disordered alloys, see, e.g., Refs. [60–62]. The analysis has demonstrated that even a high-level theory such as the CPA may fail quite badly, at least if implemented as a single-site theory. The reason for this failure is twofold: (i) Mass disorder (which is usually considered as diagonal and implemented as such in the CPA) has in fact the same effect as off-diagonal force-constant disorder, since the vibrational frequencies are determined by the interatomic force constant divided by the square root of the product of the atomic masses. (ii) Even small displacements of the atoms from their idealized lattice sites, induced by changes in the local environment, lead to pronounced changes in the local force constants. Supercell calculations, on the other hand, are in good agreement with the measured phonon frequencies and dynamical structure factors.[60,62] For dynamically stable alloys the defects of the single-site CPA could possibly be cured by a cluster version of the CPA. Ti-rich β-phase alloys, however, are dynamically unstable and the bcc lattice is stabilized only by anharmonic phonon-phonon interactions. We have therefore used the supercell approach which permits an accurate description of anharmonicity within self-consistent phonon theory. The chemical decoration of the underlying bcc or hexagonal lattices has been optimized using extensive total-energy calculations. For the low-temperature phases an unconstrained optimization of the unit-cell parameters and internal coordinates has been performed for each configuration, while for the high-temperature phase only the unit cell parameters have been relaxed at fixed reduced internal coordinates. In addition, for the bcc high-temperature phase we have used a cluster-expansion approach[53] to search for the optimal structure.

A. High-temperature bcc β Ti_3Nb alloys

1. $D0_3$-type alloys

The search for β-phase Ti alloys with optimal elastic and plastic properties has been guided by *ab initio* calculations of the elastic constants, assuming a $D0_3$ structure for Ti_3X and a B2 structure for TiX alloys.[17] These calculations predicted Ti_3Nb to be marginally stable in the $D0_3$ structure, with a very small value of the shear constants C_{44} and $C' = \frac{1}{2}(C_{11} - C_{12})$. Figure 1 compares the elastic constants of three $D0_3$-type Ti_3X alloys (X = V, Nb, and Ta) as calculated using the PAW approach implemented in VASP with the previous calculations of Ikehata *et al.*[17] based on ultrasoft pseudopotentials (USPP). The present calculations are based on very fine Brillouin-zone meshes (up to $20 \times 20 \times 20$) and use the method of LePage and Saxe[54] to extract the elastic constants from the stress-strain relations. For control some elastic constants have also been calculated using the generalized perturbation approach to the response functions, as implemented in VASP by Gajdoš *et al.*[57] Agreement of our results with Ikehata *et al.*[17] was generally very good (see Fig. 1), with the exception of C_{44} of Ti_3V and Ti_3Nb, which we found to be negative—in contrast to the previous study.

The discrepancy between the two sets of results arises from the strongly nonlinear stress-strain relation for Ti_3V and Ti_3Nb (see Fig. 2), which is in turn a consequence of a strongly structured electronic density of states in the vicinity of the Fermi level. If larger sampling strains of $\epsilon_4 \sim 4\%$ are used for the calculation of C_{44} (such as in the work of Ikehata *et al.*[17]), positive shear constants are calculated, while more accurate calculations using very small strains produce negative values (which are also confirmed by calculations using the linear response approach). For Ti_3Ta the stress-strain relation is almost perfectly linear for all strains in this range, and the

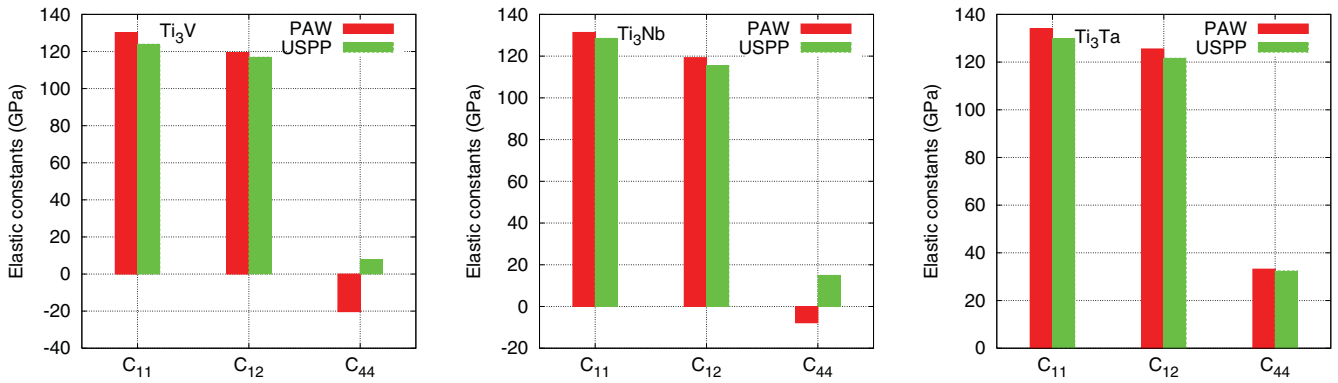

FIG. 1. (Color online) Elastic constants of $D0_3$-type Ti_3X (X = V, Nb, Ta) alloys, calculated using the PAW method and compared with the USPP calculations of Ikehata *et al.*[17] (cf. text).

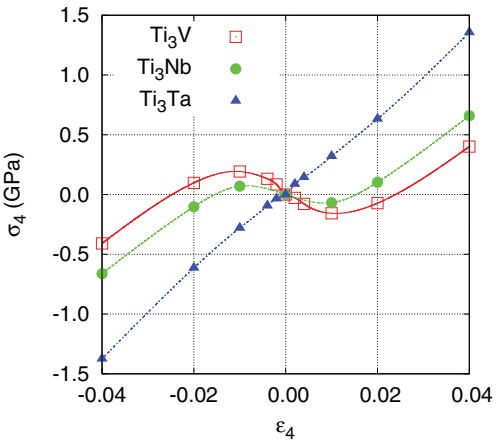

FIG. 2. (Color online) Stress-strain (σ_4 vs ε_4) relations determining the elastic shear constant C_{44} for $D0_3$-type Ti_3X (X = V, Nb, Ta) alloys (cf. text).

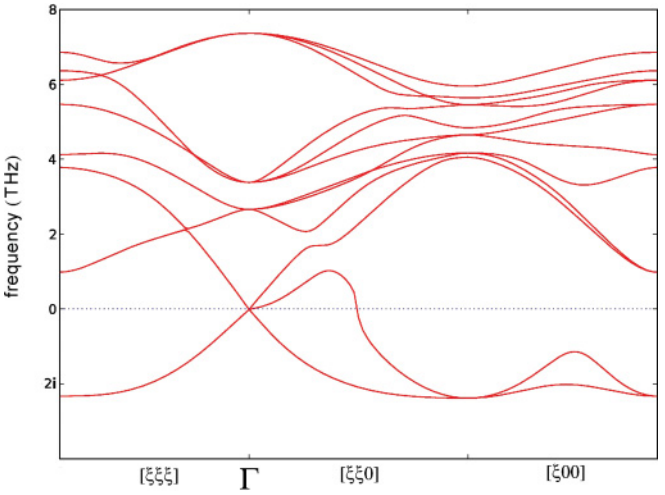

FIG. 3. (Color online) The phonon dispersion relations of $D0_3$-type Ti_3Nb, calculated in the harmonic approximation and represented in the Brillouin zone corresponding to the primitive unit cell containing four atoms (cf. text).

use of a larger sampling strain produces correct results. The difference between USPP and the all-electron PAW method is of minor importance in this case.

The formation of point defects (vacancies, antisite atoms) has been investigated using the grand-canonical formalism developed by Fähnle *et al.*[63] and applied to large supercells of $D0_3$-type intermetallic compounds by Dennler *et al.*[64] For Ti_3Nb alloys we have used large supercells consisting of $2 \times 2 \times 2$ cubic supercells containing 128 atoms. The calculations have been performed without relaxation, with relaxation at a fixed cell volume, and allowing a full relaxation of cell volume and internal coordinates. Both vacancy and antisite formations were found to be exothermic processes if a relaxation of the internal degrees of freedom was permitted. In addition, the $D0_3$ structure was found to be dynamically unstable in a harmonic approximation (the phonon dispersion calculations have been calculated using the direct method[65] and the large supercell) with imaginary acoustic phonon modes (see Fig. 3). Although the occurrence of some imaginary phonon modes was expected in an alloy undergoing a low-temperature martensitic transformation, the instability against shear deformations and the formation of point defects provide ample evidence that the $D0_3$ structure does not represent an acceptable model for these alloys. We have also investigated the possible stabilization of the structure by anharmonic phonon-phonon interactions but found that imaginary phonon modes persist to very high temperatures (see below for details). These results confront us with the necessity to construct a more suitable structural model for the β phase.

2. *Supercell models for β Ti_3Nb with an average bcc lattice*

A search for possible structures of Ti_3Nb alloys describable as superstructures of a basic bcc lattice has been conducted in a $2 \times 2 \times 2$ bcc supercell containing 16 Ti and Nb atoms in a proportion of 3 to 1. For this supercell there are 1820 different possible distributions of the two types of atoms over the available sites of the bcc lattice. However, using a group-theoretical classification 29 classes of structurally equivalent configurations can be identified. Each class consists of 4 to 192 symmetry-equivalent representatives. For all structures volume and shape of the unit cell (but not the internal coordinates, to preserve an overall body-centered lattice) have been relaxed. The calculations show that two or more classes of structures can be combined into one group—all members of this group are energetically degenerate and belong to the same space group.

Table I lists the chemical decorations, relaxed lattice constants, and atomic volume for all possible configurations of a 16-atom $2 \times 2 \times 2$ bcc supercell of Ti_3Nb. The structural energy differences are given relative to the energetically most favorable structure. The site occupation can be represented by a string of 16 binary digits—0 standing for occupation by a Ti, and 1 for occupation by a Nb atom. The notation is based on a representation of the bcc structure by two interpenetrating simple cubic lattices. The first eight digits label the sites of one, and the following eight the sites of the second lattice. Hence, e.g., the $D0_3$ structure is described by the string 0101010100000000—the first lattice is occupied alternatingly by Ti and Nb atoms, while all sites of the second lattice are occupied by Ti atoms.

The energetically most favorable structure exists in 16 different realizations (group G1); the total energy is lower by only 0.58 meV/atom than for the next favorable group of structures. Upon relaxation the cubic unit cell of these structures remains unchanged. Only for four of the 18 groups of structures (G1, G10, G14, G16) the cubic symmetry is conserved upon relaxation. Group 14 corresponds to the $D0_3$ structure, but it is found to be 7.79 meV/atom higher in energy than the energetically most favorable G1 structure. For most groups of structures, relaxation reduces the symmetry to tetragonal (groups G2–G5, G7–G9, G11–G13, G15, G17, G18); for group G6 the symmetry is only orthorhombic. Note that all tetragonal or orthorhombic distortions are very small, about 1% on average. The structure of group G18 corresponds to the well-known tetragonal $L6_0$ structure. Although this structure represents a chemical decoration with a relatively high total energy ($\Delta E \sim$ 11 meV/atom), we have found that it plays an important role in the transformation to the orthorhombic α'' phase.

TABLE I. Chemical decorations (represented by a string of 16 binary digits, cf. text), lattice constants (in Å), volume/atom Ω (in Å^3), structural energy difference ΔE relative to the energetically most favorable structure (in meV/atom) of all possible configurations of a 16-atom $2 \times 2 \times 2$ bcc supercell of a Ti_3Nb alloy. The translational symmetry is cubic (c), tetragonal (t), or orthorhombic (o), as indicated for each group of structures (cf. text).

Chem. decoration	Count	a	b	c	Ω	ΔE	Group
0000011000100100	12	6.524	6.524	6.524	17.36	0.00	G1(c)
0000110000101000	4	6.524	6.524	6.524	17.36	0.00	
0001000001000110	48	6.536	6.536	6.504	17.37	0.58	G2(t)
0111000010000000	48	6.504	6.536	6.536	17.37	0.58	
0000000010100101	24	6.561	6.459	6.561	17.38	0.76	G3(t)
0000000000010111	24	6.561	6.561	6.460	17.38	0.76	
0000000001101010	96	6.542	6.519	6.519	17.38	0.86	G4(t)
0100001010000001	48	6.512	6.550	6.512	17.36	1.44	G5(t)
0010010000101000	48	6.512	6.512	6.550	17.36	1.44	
0000100011000001	192	6.497	6.528	6.554	17.37	1.54	G6(o)
0100100110000000	48	6.520	6.520	6.538	17.37	1.62	G7(t)
0001110010000000	48	6.520	6.520	6.538	17.37	1.62	
0110000000100010	96	6.538	6.538	6.502	17.37	2.33	G8(t)
0100100000100010	24	6.512	6.556	6.512	17.37	2.38	G9(t)
1001000000100100	24	6.512	6.512	6.556	17.37	2.38	
1001101000000000	32	6.526	6.526	6.526	17.37	2.51	G10(c)
0000100001110000	96	6.526	6.526	6.526	17.37	2.51	
0011100010000000	96	6.518	6.518	6.535	17.36	3.60	G11(t)
1010000001000010	96	6.355	6.518	5.518	17.36	3.60	
0001100001000001	192	6.535	6.518	6.518	17.36	3.60	
0010000100100001	96	6.556	6.456	6.556	17.36	4.18	G12(t)
1001000010001000	192	6.556	6.556	6.465	17.36	4.18	
0001000100000011	96	6.556	6.465	6.556	17.36	4.18	
0001000100100001	12	6.583	5.915	6.583	17.36	6.26	G13(t)
0101010100000000	4	6.522	6.522	6.522	17.34	7.79	G14(c-$D0_3$)
0100000001100001	48	6.558	6.558	6.445	17.33	9.86	G15(t)
0001010100000001	16	6.521	6.521	6.521	17.33	10.41	G16(c)
1000100000000110	48	6.545	6.507	6.507	17.32	11.22	G17(t)
0010100010001000	12	6.499	6.499	6.561	17.32	11.38	G18(t-$L6_0$)

The energetically most favorable G1 structure has space-group symmetry $R\bar{3}m$. The lattice constant is $a = 6.524$ Å for the $2 \times 2 \times 2$ bcc supercell containing 16 atoms. The lattice constant of $a_{bcc} = 3.262$ Å for the underlying bcc lattice is almost identical with the results of Ikehata *et al.*[17] (3.273 Å) and Sun *et al.*[28] (3.260 Å), assuming a $D0_3$-type ordering and with the room-temperature measurements of Kim *et al.*[10] ($a_{bcc} = 3.287$ Å). A schematic representation of the three most relevant structures is shown in Fig. 4. The G1 structure is characterized by chains of nearest-neighbor Nb atoms running along one of the body diagonals, e.g., the [111] directions. In the $D0_3$ structure chains of Nb atoms extend along the face diagonals. In the tetragonal $L6_0$ structure chains of Nb atoms are arranged parallel to one of the edges of the cell. The essential difference between the alloy models is evident: Whereas in the $D0_3$ structure each Nb atom has eight Ti neighbors in the first and six Ti neighbors in the second coordination shell, in the G1 structure the Nb atoms have two Nb and six Ti next and six Ti next-nearest neighbors, and in the $L6_0$ structure the Nb atoms have eight Ti next and four Ti and two Nb next-nearest neighbors. Similar arrangements of nearest-neighbor Nb-Nb bonds as for the G1 structure, in the form of zigzag or spiral chains, are also characteristic for other low-energy structures, emphasizing the importance of strong Nb-Nb interactions for the structural stability. All three structures may also be described by smaller primitive unit cells containing only four crystallographically inequivalent atoms, as shown in Fig. 4.

The energetic ordering changes if different levels of relaxation are permitted. A relaxation of the internal coordinates at a fixed cell shape and under the constraint of conserving space-group symmetry (which is the standard mode of relaxation in VASP) leaves the G1, $D0_3$, and $L6_0$ structures unchanged. If prior to the relaxation of the atomic positions the symmetry is broken, the energy of the G1 structure is lowered by 9.4 meV/atom, that of the $L6_0$ phase by 14.5 meV/atom. The $D0_3$ structure remains unchanged. A subsequent full relaxation (volume and shape of the unit cell and internal coordinates) lowers the energy of the G1 phase further by 6.7 meV/atom and that of the $L6_0$ phase further by 14.3 meV/atom. Hence the fully relaxed $L6_0$ structure is lower in energy by 25 meV/atom than the $D0_3$ phase and by 1.2 meV/atom lower than the G1 phase. As we demonstrate below, it represents a possible model for transforming to the α'' phase. The structure resulting from a fully unconstrained relaxation of the G1 structure, on the other hand, represents only a local minimum of the potential energy and was found to be dynamically unstable. This is a first indication that upon transformation to a more stable

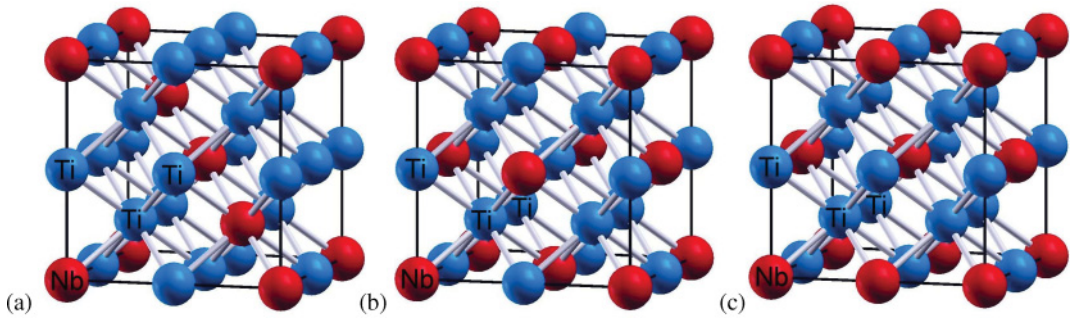

FIG. 4. (Color online) Comparison of the chemical decoration of the $2 \times 2 \times 2$ bcc supercell of a Ti_3Nb alloy corresponding to the G1 (a), $D0_3$ (b), and $L6_0$ (c) structures. Ti atoms are shown in blue (light gray), Nb atoms in red (dark gray). For all three structures an irreducible four-atom unit cell may be defined. The crystallographically inequivalent sites in the irreducible cell are labeled by the chemical symbols (cf. text).

low-temperature phase the chemical decoration optimized for the bcc lattice will not be conserved.

We have also calculated the elastic constants for the G1 β-phase Ti_3Nb alloy, and the results are compiled in Table II together with the elastic constants measured by Takesue *et al.*[23] and by Talling *et al.*[26,27] for different gum-metal specimens. For these alloys the electron/atom ratio lies in the range between 4.25 and 4.26. These values are very close to $e/a = 4.25$ for Ti_3Nb. For the ground-state structure and under applied constant strain the coordinates of all atoms within the 16-atom supercell have been relaxed under the constraint of conserving space-group symmetry. The results show that in contrast to the $D0_3$-type alloy, G1-type Ti_3Nb is stable against shearing. By construction, at low temperatures the G1 phase is also stable against the formation of antisite defects.

The elastic constants of gum-metal have been determined by Takesue *et al.*[23] by a Monte Carlo fitting procedure from the moduli determined by compressive and tensile tests on single-crystal specimens. Talling *et al.*[26,27] used synchrotron x-ray diffraction on specimens produced from elemental powders (EPs) by the same techniques as those used by Takesue *et al.*, as well as specimens of identical composition but prepared using a different technique (plasma spraying and hot pressing—HP).

The comparison with experiment demonstrates that the G1-type Ti_3Nb alloy has elastic shear constants which are very similar to those measured for gum-metal alloys. Calculations of the phonon dispersion relations in the harmonic approximation confirm that all acoustic phonons have real eigenfrequencies. However, the G1 structure has imaginary optical phonon modes, similar to bcc Ti, which can be stabilized only by anharmonic phonon-phonon interactions. Details of the harmonic and anharmonic phonons in the β phase of Ti_3Nb will be discussed together with the temperature-driven phase transformation.

In the following we assume that the G1-ordered binary alloy is a good model system for the high-temperature phase of gum-metal alloys. However, this does not mean that we claim that the β phase is an ordered intermetallic compound. First, the G1 structure is only one among sixteen symmetry-equivalent and energetically degenerate configurations. A real alloy will consist of a disordered arrangement of domains consisting of these 16 configurations. Second, the energy differences between the various ordered structures representing different chemical decorations are sufficiently small such that low-energy configurations can be realized at a local level, the increase in internal energy being compensated by a gain in configurational entropy. However, for calculation of the dynamical properties we need a supercell model which is stable at least against shear deformations. This condition is fulfilled for the G1 structure.

TABLE II. Elastic constants (in GPa) calculated for bcc $D0_3$- and G1-type Ti_3Nb alloys, compared with experimental results measured on gum-metal specimens of slightly different compositions (cf. text).

Alloy	C_{11}	C_{12}	C_{44}	C'	Reference
Theory					
Ti_3Nb (G1)	148.8	111.4	37.5	18.7	PW[d]
Ti_3Nb ($D0_3$)	131.3	119.3	−7.8	6.0	PW[d]
Ti_3Nb ($D0_3$)	128.5	115.5	14.9	6.5	17
Ti_3Nb ($D0_3$)	117.3	105.6	19.9	5.8	28
Experiment					
Ti-23Nb-0.7Ta-2Zr-O[a]			28.5–35.6	12.3–13.7	23
EP[b]	125	93	28	16	26
HP[c]	125	90	31	17.5	26

[a]Composition given in atomic percent (cf. text).
[b]Produced from elemental powders and cold pressing.
[c]Produced by plasma spraying and hot pressing.
[d]Present work.

3. Cluster expansion calculations for bcc Ti-Nb alloys

In order to make an exhaustive search for concentration-dependent ground-state structures based on a given lattice, the cluster expansion (CE) technique was applied by exploiting the capabilities of the Universal Cluster Expansion code UNCLE.[66]

The key concept of CE is to describe the infinite solid as a set of interacting clusters of atoms located on the sites of a lattice and to reformulate the total energy in terms of a cluster series.[53] For a binary A_xB_{1-x} alloy, the enthalpy of formation $\Delta H(\sigma_i)$ for a given distribution σ_i of the A and B atoms over the sites of the crystal lattice is given by

$$\Delta H(\sigma_i) = E(A_xB_{1-x},\sigma_i) - xE(A) - (1-x)E(B). \quad (3)$$

The enthalpy of formation is linearly expanded into a sum of energies characteristic for geometrical building blocks (single atoms, dimers, triangles, etc.) of the structure, similar to a Heisenberg model of interacting spins,

$$\Delta H(\sigma_i) = \sum_F D_F \Pi_F(\sigma_i) J_F, \quad (4)$$

in which the coefficients D_F and the correlation functions $\Pi_F(\sigma_i)$ are determined by the geometry of the underlying crystal lattice and its chemical decoration in the configuration σ_i. The so-called effective cluster interaction energies J_F are determined by fitting formation energies of a suitably selected set of structures derived by a DFT method (such as VASP) to the expansion in Eq. (4). Making use of UNCLE, structures for compounds are constructed for which DFT formation energies are evaluated. From these a set of cluster interaction energies J_F are derived which are then used (i) to test the fit to the input DFT structures and (ii) to predict formation energies for new ground-state structures which are then recalculated by DFT. This procedure is repeated until a sufficient set of figures and corresponding cluster interaction energies are obtained from which energies of formation are determined according to Eq. (4), which fit all DFT energies within a cross-validation score of 0.5 meV (for the present case of bcc Ti-Nb alloys) with respect to formation energies per atom. Now, this converged CE is used to find the most stable structures, i.e., the ones with lowest formation energies which constitute the ground-state line of the concentration-dependent phase diagram.

Normally, the total energy calculations are performed for fully relaxed structures to account for local distortions of the lattice depending on the given chemical decoration. However, for the metastable high-temperature phase of Ti-Nb alloys, only the volume of the unit cell can be allowed to relax, because an optimization of the cell shape and the internal degrees of freedom could eventually relax to the more stable low-temperature phase or to an intermediate metastable phase of different symmetry.

CE calculations for the bcc β phase of Ti-Nb alloys have been performed for the entire concentration range. To create the final input for the calculation of the cluster interactions, total energies have been calculated for 95 different structures, including at the composition Ti_3Nb three structures with four inequivalent sites per primitive unit cell (i.e., the G1, $D0_3$, and $L6_0$ structures) and three structures with eight sites per primitive unit cell. For these structures only the volume of the unit cell has been relaxed; the shape of the unit cell and the internal positions of the atoms have been kept frozen. With the cluster interactions determined from these data, altogether 163 373 structures with up to 16 atoms per primitive unit cell may be generated, including 3450 structures with the composition Ti_3Nb. Details of the CE calculations will be reported elsewhere;[67] here the important point is that the CE calculations predict and confirm that at the composition Ti_3Nb the G1 structure indeed has the lowest energy of all 3450 structures investigated on a bcc lattice.

B. Supercell models for the low-temperature α' phase of Ti_3Nb

The α' phase of the Ti-rich alloys is in principle a solid solution of the second component in the hexagonal low-temperature phase of Ti. Hence at the composition Ti_3Nb this phase will be strongly supersaturated with Nb. However, for completeness it has been included in our analysis. To construct a model for the α' low-temperature phase of Ti_3Nb we have followed a strategy similar to that used for the bcc phase. We constructed a supercell containing 16 atoms based on the hexagonal B_h lattice. The lower symmetry of this structure made it necessary to reduce the number of possible configurations by fixing the occupation of one half of the lattice sites with Ti, but this still leaves 66 different decorations of the basic B_h structure. For these low-temperature structures we have performed a complete relaxation of the volume and shape of the supercell and also of all atomic coordinates. According to their energies, the structures can be arranged into ten groups (some of them turn out to be energetically degenerate), and for three of these groups the internal energy is lower than for the high-temperature bcc G1 phase. The first two energetically degenerate groups contain 16 and 8 structures with monoclinically distorted cells and a strong Nb-Nb interaction. These structures are by about 10 meV/atom energetically more favorable than the G1 phase. The third group consists of four monoclinic structures and is about 3 meV/atom higher in energy than the structures from the first two groups. The site occupation of these structures is closely related to that from the first two groups, but they differ in the absence of the nearest-neighbor Nb-Nb interactions. Representative examples from all three groups are shown in Fig. 5. The energetically degenerate fourth and fifth groups of structures are already higher in energy than the G1 structure and have a tetragonal unit cell. For these five groups of structures the information on the chemical decoration, lattice parameters, and total energies is compiled in Table III.

The other groups of structures have higher energy than the G1 structure and are therefore not suitable candidates for a martensitic phase. It should be noted that the hexagonal symmetry is preserved upon relaxation only for the six structures with the highest energies, which are by 17 meV/atom less favorable than the bcc G1 phase. By construction these relaxed structures are at least metastable with respect to elastic deformations and the formation of antisite point defects.

For the structures from groups H1, H2, and H3 we have also calculated the phonon dispersion relations in a harmonic approximations. Imaginary phonon modes have been found for those from groups H1 and H2. These structures are therefore unsuitable as models for a metastable low-temperature phase

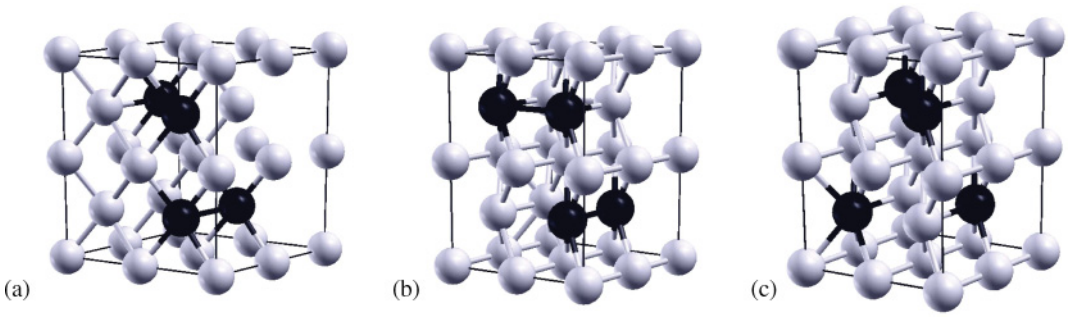

FIG. 5. (Color online) Supercells containing 16 atoms of the energetically most favorable groups of structures produced by relaxation of a B_h structure with different chemical decorations used to model the α' phase: structures from groups H1 (a), H2 (b), and H3 (c). Ti atoms are shown in gray, Nb atoms in black (cf. text).

derived from an hcp structure. In contrast, for structure H3 all eigenmodes are found to be real; the structure is found to be dynamically stable (see Fig. 6). This structure is a possible candidate for the metastable low-temperature α' phase of Ti_3Nb. The distortion from the basic hexagonal lattice is caused by the large content of Nb, which makes this structure also less stable than the orthorhombic α'' and hexagonal ω phases (see below).

C. Structure of orthorhombic α″ Ti_3Nb martensite

The α'' martensite has an orthorhombic lattice[3,68–70] with the atoms in positions arranged according to space group $Cmcm$. The Wyckoff positions are (0,0,0), (1/2,1/2,0), $(0,1-2y,1/2)$, and $(1/2,1/2-2y,1/2)$, with y being ≈0.2. By varying b/a, c/a, and y the hcp structure of the α' phase (for $b/a=\sqrt{3}, c/a=\sqrt{8/3}, y=1/3$) and the bcc structure of the β phase (for $b/a=\sqrt{2}, c/a=\sqrt{2}, y=1/4$) may be produced. Lattice constants of the α'' phase of Ti-Nb alloys with 15 − 35 at. % Nb have been reported by Kim *et al.*[10] At the composition Ti_3Nb the measured lattice constants are $a=3.19$ Å, $b=4.80$ Å, and $c=4.64$ Å. The orthorhombic structure may be viewed as arising from a distortion of a supercell containing four atoms inscribed to the bcc lattice of the β phase and a slight displacement of the atoms decorating the faces of the new unit cell (see Fig. 7).

As for the β phase, the chemical decoration of the orthorhombic lattice remains to be specified. In their calculations of the elastic constants of α'' Ti_3Nb, Sun *et al.*[28] had assumed that the $(1/2,1/2-2y,1/2)$ site is occupied by Nb without investigating alternative decorations. The two crystallographically inequivalent sites allow only two different chemical decorations. Our calculations show that the decoration assumed by Sun *et al.*[28] is the most stable one, but both allowed decorations differ by only 0.005 meV/atom in energy. If the optimized structure of the α'' martensite is transformed back to the bcc lattice, the chemical decoration corresponds to the $L6_0$ structure.

Our starting points for the construction of models for the α'' phase were hence the chemical decorations of the bcc lattice in the G1 and $L6_0$ structures, described in the rotated coordinate system appropriate to the α'' phase (see Fig. 7). A relaxation at constant cell volume and fixed lattice parameter b, but without any symmetry constraints (the symmetry must be broken in the initial configuration), has been performed using the GADGET routine.[52] The relaxation lowers the total energy of the G1 structure by ∼7.5 meV/atom and that of the $L6_0$ structure by ∼22 meV/atom. While the relaxed G1 structure is stable against a distortion along the (110) direction required to match the orthorhombic α'' structure, the distortion of the relaxed $L6_0$ lattice lowers the total energy by a further ∼6.8 meV/atom (see Fig. 8). A stable energy minimum is reached for the orthorhombic lattice parameters, 3.34, 4.77, and 4.41 Å, and a value of the internal parameter of $y=0.20$, in good agreement with the experimental lattice constants reported by Kim *et al.*[10] and those calculated by Sun *et al.*[28] According to our calculation, the total energy of the α'' structure is by 17.4 meV/atom lower than that of the bcc G1 structure and lower by 1.2 meV/atom than the distorted structure resulting from an unconstrained relaxation

TABLE III. The five groups of possible Ti_3Nb structures with a total energy lower or comparable to that of the bcc G1 structure. These structures have been created by decorating the sites in a 16-atom supercell of the B_h lattice and full relaxation. The chemical decoration is described by a string of 16 binary digits, 0 standing for the occupation with Ti, 1 with Nb atoms. Lattice constants are given in Å, volume/atom in Å^3, and angles in degree. The energy difference ΔE (in meV/atom) has been evaluated relative to the most stable bcc phase (the unrelaxed G1 structure) (cf. text).

Chem. decoration	Count	a	b	c	α	β	γ	Volume	ΔE	Group
0000000010010011	16	5.797	6.612	8.900	90	90	55.2	17.51	−9.7	H1
0000000001001110	8	5.797	5.797	8.897	90	90	69.6	17.51	−9.7	H2
0000000010011001	4	6.758	5.827	8.734	90	90	54.6	17.51	−7.0	H3
0000000011100010	16	9.164	6.511	6.586	90	90	45.3	17.45	+2.7	H4
0000000011010100	8	6.512	6.512	6.586	90	90	89.4	17.45	+2.7	H5

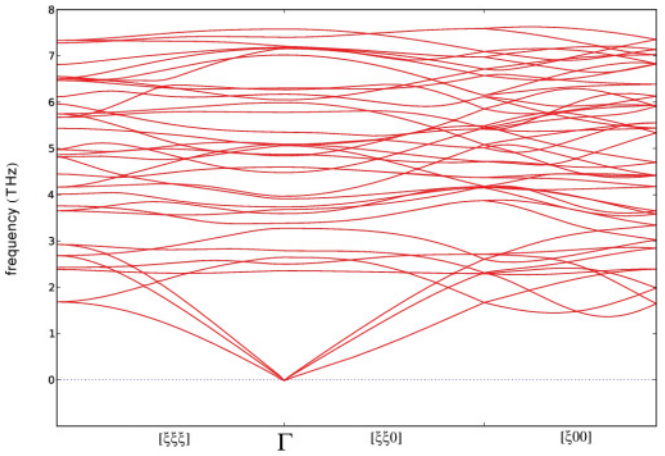

FIG. 6. (Color online) The phonon dispersions of α' Ti_3Nb in the H3 structure, calculated in the harmonic approximation and shown in the Brillouin zone corresponding to the 16-atom cell (cf. text).

of the G1 structure. It is also considerably lower than any of the structures based on the relaxed hexagonal B_h lattice. The higher stability of the α'' phase is consistent with experimental observations. However, it is important to emphasize that although the bcc lattice of the β phase may be continuously deformed to the orthorhombic α'' phase, the optimal chemical decoration of both lattices is different; a phase transformation will hence involve changes in the site occupation. In fact, the structural relation with the $L6_0$ structure has been discovered by following the inverse transformation from the α'' to the β phase.

We have also calculated the elastic constants of the optimized α'' phase and the results are compiled in Table IV.

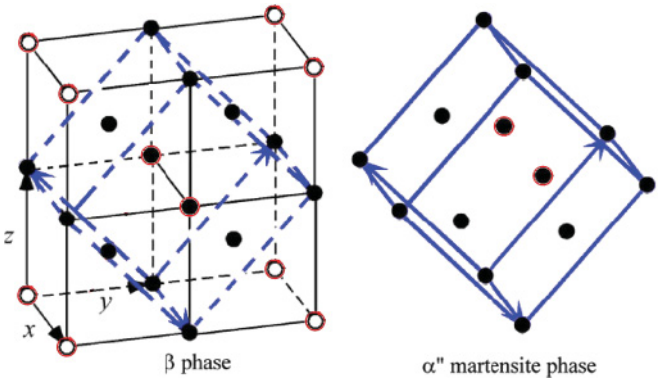

FIG. 7. (Color online) Schematic illustration of the structural relationship between the bcc β and the orthorhombic α'' phases of Ti_3Nb. The α'' phase may be generated by a shear deformation of a supercell inscribed into the bcc lattice and a slight displacement of the atoms decorating the faces of this cell. The chemical decoration is shown for the $L6_0$ structure. In this case relaxation of the internal coordinates, followed by an orthorhombic distortion of the inscribed supercell, yields immediately to the α'' structure with the chemical decoration giving the lowest energy. Ti atoms are represented by black balls, Nb atoms are marked by red circles around the black dots (cf. text).

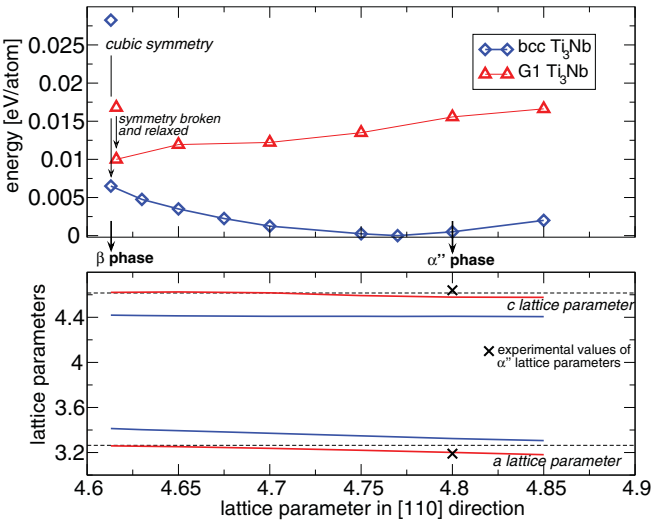

FIG. 8. (Color online) Variation of the total energy of the G1 (red triangles) and $L6_0$ (blue diamonds) models of the β-phase structure upon relaxation of the internal coordinates at fixed cell shape (after breaking point group symmetry) and further distortion along the (110) direction to induce a transformation to the orthorhombic α'' phase. Note that the distortion of the relaxed $L6_0$ structure leads to a stable orthorhombic structure, whereas the distortion is energetically unfavorable for the relaxed G1 structure (cf. text).

The conditions for the elastic stability of the orthorhombic lattice are[71]

$$\begin{aligned} C_{ii} &> 0 \quad \text{for} \quad i = 1-6, \\ C_{22}C_{33} - C_{23}^2 &> 0, \\ C_{11}C_{22}C_{33} + 2C_{12}C_{13}C_{23} - C_{12}^2C_{33} - C_{13}^2C_{22} - C_{23}^2C_{11} &> 0, \end{aligned} \tag{5}$$

and they are all satisfied for the fully relaxed structure. Compared to the elastic constants calculated by Sun *et al.*,[28] we find considerably higher values for all shear constants.

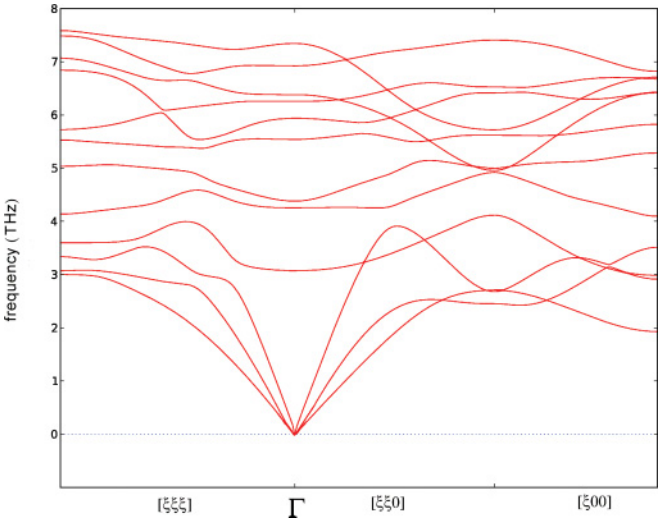

FIG. 9. (Color online) Phonon dispersions of orthorhombic α'' Ti_3Nb along the principal symmetry directions, calculated in the harmonic approximation and represented in the Brillouin zone corresponding to the orthorhombic four-atom elementary cell.

TABLE IV. Elastic constants (in GPa) calculated for orthorhombic α'' Ti_3Nb alloy (cf. text).

Alloy	C_{11}	C_{12}	C_{13}	C_{22}	C_{23}	C_{33}	C_{44}	C_{55}	C_{66}	Reference
Ti_3Nb	148.1	93.0	123.8	171.1	80.4	174.6	64.7	44.9	32.3	PW[a]
Ti_3Nb	129.9	91.1	126.8	148.2	69.3	135.6	28.4	23.1	39.7	[28]

[a]Present work.

The phonon dispersion relations of orthorhombic α'' Ti_3Nb calculated in the harmonic approximation for the irreducible four-atom cell are shown in Fig. 9. All eigenmodes are found to be real—the structure is elastically and dynamically stable. Hence the structure represents an acceptable model for the low-temperature phase. However, it must also be noted that the relation between the bcc G1 and the orthorhombic α'' structures is not quite as simple as suggested for a completely random alloy—the optimal model for the α'' structure has been derived from a bcc lattice with a slightly different chemical decoration than the optimized G1 model of the β phase.

D. Structure of the low-temperature ω phase of Ti_3Nb

The ω phase of Ti-based alloys exists in two slightly different modifications—hexagonal and trigonal.[5] The hexagonal version has the AlB_2-type structure with space group $P6/mmm$ and three atoms per unit cell at positions (0,0,0), (2/3,1/3,1/2), and (1/3,2/3,1/2), the axial ratio is $c/a \sim 0.62$. The structure may be considered as an ABAB... stacking sequence of triangular A and honeycomb B layers. The structure may be derived from the bcc structure by collapsing one pair of (111) planes to the intermediate position, creating a honeycomb layer, leaving the next plane unchanged, and collapsing the next pair and so forth [see Fig. 10(a)]. The complete collapse (atomic displacements by $\pm a_{bcc}\sqrt{3}/12$) will produce the ideal ω structure with $a_\omega = \sqrt{2}a_{bcc}$ and $c_\omega = \sqrt{3}a_{bcc}/2$. Displacements smaller than $a_{bcc}\sqrt{3}/2$ from the positions in the bcc phase will lead to the formation of the trigonal ω phase (sometimes also referred to as the "rumpled" ω structure). The space group is $P\bar{3}m1$, and atoms are located at positions (0,0,0), $(2/3,1/3,1/2+z)$, and $(1/3,2/3,1/2-z)$. The hexagonal ω structure corresponds to $z = 0$. The bcc structure is recovered for $z = 1/6$ and $c/a = \sqrt{3/8}$.

The elementary cell of the ω structure contains only three atoms. The smallest supercell compatible with the stoichiometry Ti_3Nb contains 12 atoms. Starting from the G1 structure of the β phase, the collapse model leads after relaxation to a hexagonal ω structure with a lattice constant of $a_\omega = 9.324$ Å and an axial ratio of $c/a = 0.30$ for the supercell. For the primitive hexagonal cell, the lattice constant of 4.66 Å and the axial ratio of 0.30 are in perfect agreement with the results of Sun *et al.*[28] The structure of the ω phase, with the chemical decoration derived from the G1 structure, is shown in Fig. 10(b). The total energy is 10 meV/atom lower than for the G1-type β phase, but higher by 7.4 meV/atom than for the α'' structure. Note that the structure of the ω phase can be derived from the G1 structure of the β phase without any change of site occupation.

The elastic constants for the ω phase are compiled in Table V. They are in reasonable agreement with the results of Sun *et al.*[28] The conditions for the elastic stability of the hexagonal structure[71]

$$\begin{gathered} C_{44} > 0, \\ (C_{11} + C_{12})C_{33} - 2C_{13}^2 > 0, \\ C_{11} - C_{12} > 0, \end{gathered} \tag{6}$$

are all satisfied and the hexagonal ω structure is elastically stable.

A calculation of the phonon dispersion relations in the harmonic approximation confirms that all acoustic modes are stable but display an imaginary long-wavelength optical mode along the [$\xi\xi$0] direction (see Fig. 11). The eigenvectors of this mode show that it consists of a displacement of the Nb atoms located in the collapsed honeycomb-type layer perpendicular to the plane. A static relaxation without the constraint of hexagonal symmetry, however, does not converge to a trigonal phase where pairs of atoms are displaced in opposite directions.

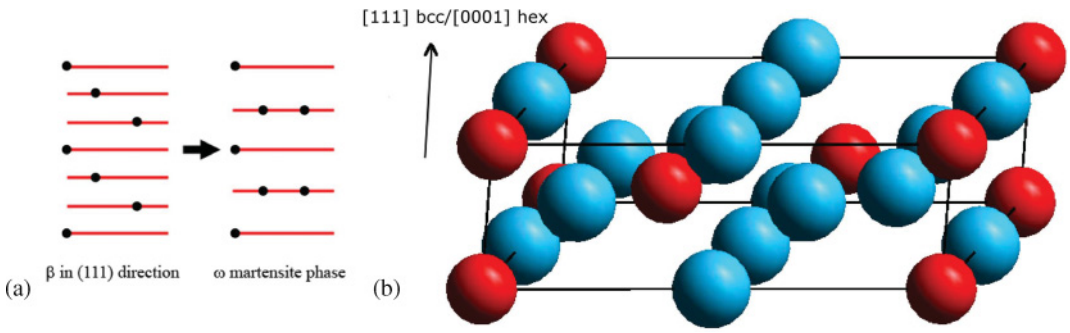

FIG. 10. (Color online) (a) Schematic representation of the collapse model for the relation between the structural models of the bcc β and hexagonal ω phases. (b) Supercell containing 12 atoms representing the structure of the hexagonal ω Ti_3Nb alloys. The [111] direction of the bcc lattice corresponds to the [0001] axis of the hexagonal lattice. Ti atoms are shown in blue (dark), Nb atoms in red (light gray) (cf. text).

TABLE V. Elastic constants (in GPa) calculated for hexagonal ω Ti_3Nb alloy, cf. text.

Alloy	C_{11}	C_{12}	C_{13}	C_{33}	C_{44}	C_{66}	Reference
Ti_3Nb-hexagonal	226.0	116.7	80.7	276.4	54.7	38.8	PW[a]
Ti_3Nb-hexagonal	162.2	124.9	84.8	234.3	22.3	18.6	[28]

[a]Present work.

This suggests that this mode will be stabilized by modest anharmonic corrections. A self-consistent phonon calculation for such a large cell with low symmetry, however, turns out to be computationally very demanding. Therefore, the calculation of the vibrational free energy for the ω phase has been performed in the harmonic approximation and the contribution of the soft mode has been set to zero.

IV. STABILIZATION OF THE bcc β PHASE BY ANHARMONIC INTERACTIONS

In the preceding sections we have constructed structural models for the β, α', ω, and α'' phases of Ti_3Nb alloys. Relative to the most stable α'' phase the structural energy differences are 7.4, 10.4, and 17.4 meV/atom for the ω, α', and β phases, respectively. While the relaxed structures of the α'' and α' phases have been shown to be both elastically and dynamically stable, and the ω phase shows only one imaginary phonon mode related to displacements of the Nb atoms from the collapsed honeycomb plane, the optimized G1 structure of the β phase was found to be elastically stable but dynamically unstable, with imaginary optical phonon modes extending over almost the entire Brillouin zone. To verify that, as for the β phase of pure Ti, the G1 structure is stabilized already at moderate temperatures by anharmonic interactions, the phonon dispersion relations have been calculated using self-consistent phonon theory as implemented in the SCAILD method for temperatures up to 1600 K. Figure 12 shows the phonon dispersion relations calculated in the harmonic

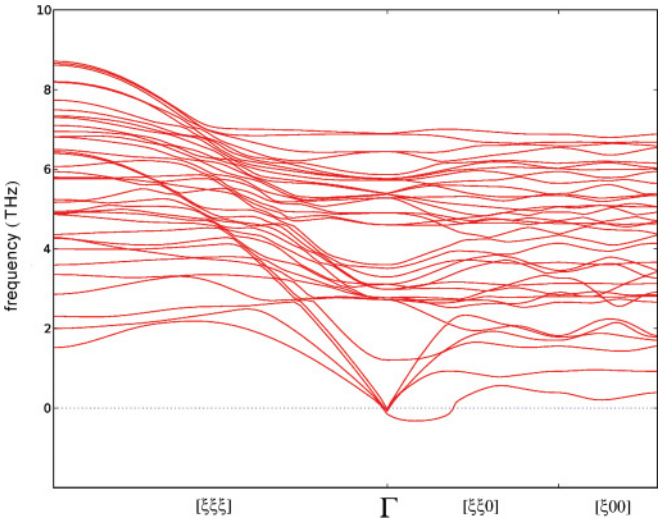

FIG. 11. (Color online) The phonon dispersion relations of the hexagonal ω phase Ti_3Nb alloy along the principal symmetry directions of the Brillouin zone corresponding to the hexagonal supercell with 12 atoms, calculated in the harmonic approximation.

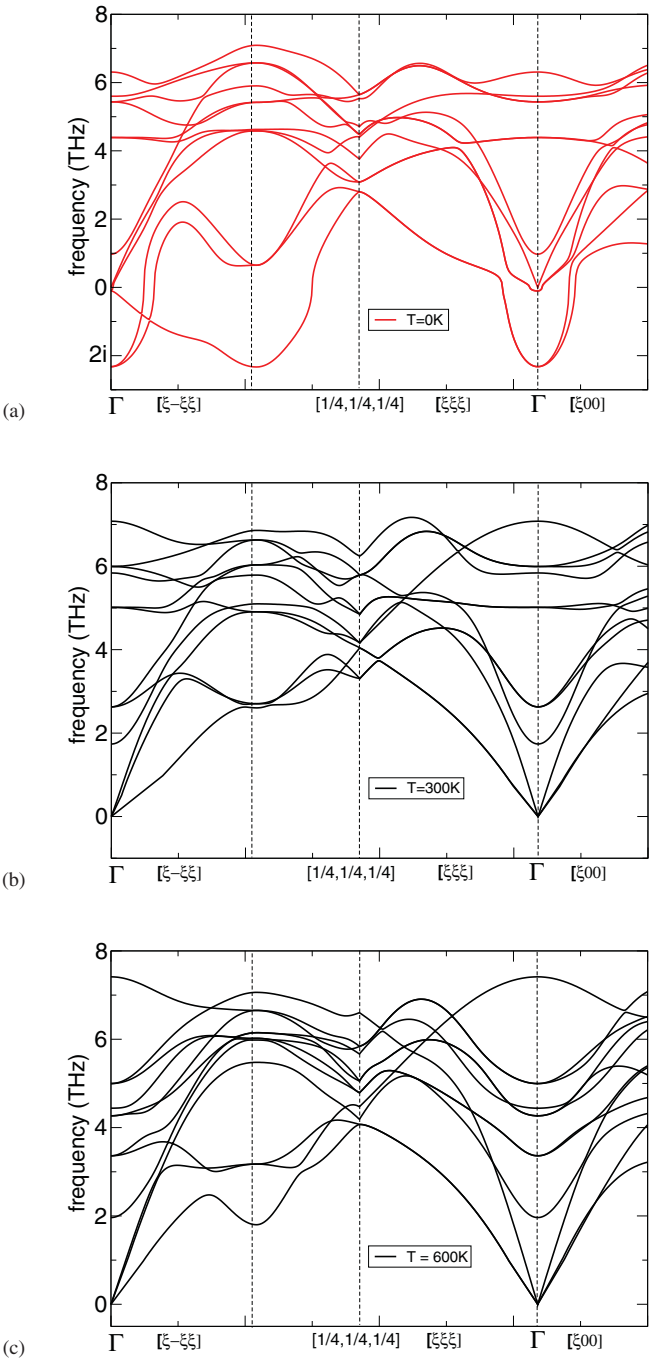

FIG. 12. (Color online) The phonon dispersions of the β Ti_3Nb alloy in the G1 structure, calculated in the harmonic approximation (a) and using self-consistent phonon theory at $T = 300$ K (b) and $T = 600$ K (c). The dispersion relations are drawn for the Brillouin zone corresponding to the irreducible four-atom elementary cell.

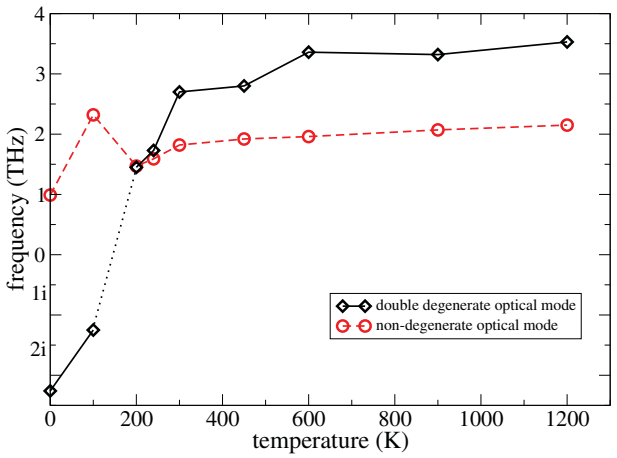

FIG. 13. (Color online) Temperature dependence of the soft optical mode (black diamonds) and of the lowest stable (nondegenerate) optical mode (red circles) at the Γ point for the G1 structure of the β phase of Ti_3Nb.

approximation and using self-consistent phonon theory at temperatures of 300 K and 600 K. We find that already at room temperature the anharmonic phonon-phonon interactions stabilize the soft optical modes.

The dynamical instability of the β phase is driven by the softening of the optical mode at the Γ point which occurs in a narrow temperature interval between 200 and 100 K (see Fig. 13). A similar sudden jump in the frequency of a transverse acoustic phonon has been reported for the self-consistent phonon calculations for B2-type Ni-Ti alloys by Souvatzis *et al.*[38] It has been argued that the discontinuous variation of the frequency is a consequence of the relatively small size of the supercell, since this leads to an overestimation of the contributions of different phonon modes to the atomic displacements, especially at very low frequency. For a larger supercell with an increased number of commensurate phonons, a more continuous variation of the soft-mode frequency is expected. However, the important point is that the $\beta \rightarrow \alpha''$ or $\beta \rightarrow \omega$ transitions occur already at higher temperatures (see below). In contrast to the soft optical modes, the other phonon modes show only a much weaker temperature dependence. As an example, the variation of the lowest stable optical mode at the Γ point is also shown in Fig. 13.

To confirm our choice of the G1 structure for the model structure of the β phase, we have also applied the self-consistent phonon method to the $D0_3$ structure. In this case, the acoustic shear modes corresponding to the negative C_{44} shear constant and several optical modes are imaginary over the largest part of the Brillouin zone. For the $D0_3$ structure the anharmonic interactions cannot stabilize the soft eigenmodes—imaginary eigenfrequencies are calculated for temperatures up to 1200 K. The dramatic differences between the anharmonic phonon spectra of the G1 and $D0_3$ structures demonstrate the decisive influence of the chemical decoration of the basic bcc lattice for the stabilization of the β phase.

V. TEMPERATURE-DRIVEN PHASE TRANSITIONS

The phase stable at a given temperature T is determined by the minimum free energy, including vibrational and electronic contributions to the entropy. Phases that are only metastable or even unstable at low temperatures may be favored at higher temperatures by a larger entropy, leading to a lower free energy. In principle, this requires calculation of the vibrational spectra and free energies of all competing phases at the same level of theory. For the bcc β phase, which is dynamically unstable, anharmonic effects must be included—here via a self-consistent phonon approach. As we have mentioned, up to 100 iterations are required to achieve self-consistency even for the highly symmetric bcc β phase. For the low-symmetry orthorhombic, hexagonal, or monoclinic relaxed structures of the low-temperature phases, such calculations will be almost prohibitively demanding. On the other hand, the results for the β phase demonstrate that for the modes stable already in a harmonic approximation, anharmonic effects tend to be modest. This suggests use of the harmonic approximation for the dynamically stable phases for calculating the temperature dependence of the free energy. Another difficult point is to account for the effect of thermal expansion. In principle this requires calculation of the phonon spectra and the vibrational free energy at each temperature at different volumes and minimization of the free energy as a function of temperature. The alternative is to neglect thermal expansion and to perform the calculations at fixed volume.

To test the validity of these simplifying assumptions we have calculated the martensitic transition temperature of pure Ti. The structural energy difference between the bcc and hcp phases of Ti is 114 meV/atom according to our calculation. Calculation of the vibrational free energy $F_{\mathrm{vib}}(V,T)$ has been performed for bcc Ti using the self-consistent phonon approach as implemented in SCAILD, while for hcp Ti the calculation has been performed in the harmonic approximation. The calculations for both phases have been performed at fixed atomic volume, as calculated at $T = 0$ K. The variation of the free energy and of the contributions from the vibrational and electronic entropies are shown in Fig. 14(a). This approach predicts a martensitic transition temperature of $T_c = 1300$ K, to be compared with an experimental value[30] of $T_c = 1155$ K. In order to investigate the influence of thermal expansion, we evaluated the total free energy $F(V,T)$ as a function of volume at a fixed temperature of $T = 1200$ K. The thermal expansion of 0.006% leads to a reduction of the difference in the vibrational free energies by about 12 meV and results in a decrease of the calculated transition temperature by $\approx$120 K, giving the transition temperature of Ti in almost perfect agreement with experiment. Hence, the same simplifications—harmonic approximation for the low-temperature phases and constant volume—have also been used for estimating the transition temperatures between the different phases of Ti_3Nb alloys.

Figure 14(c) shows calculated free-energy differences between the β and α'' phases of Ti_3Nb as a function of temperature. The difference in the internal energies of the α'' and β phases is 17.4 meV/atom. The free-energy difference is lower already at low temperatures because of a significant differences in the zero-point vibrational energies favoring the β phase. We also find a higher electronic entropy for the β phase because of a higher density of states at the Fermi level. Above a temperature of about 700 K the β phase is lower

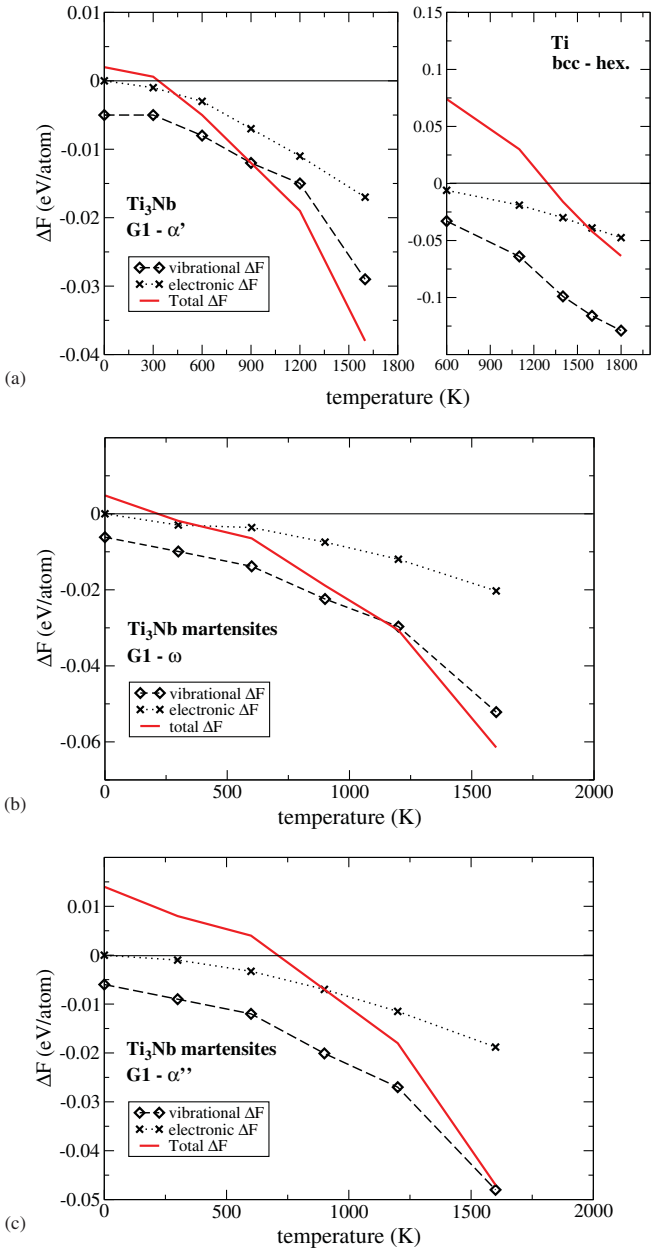

FIG. 14. (Color online) The free-energy differences (red line) between the G1-type β phase of Ti_3Nb and the stable low-temperature phases: (a) α' (including for comparison also the free-energy difference between the β and α phases of pure Ti), (b) hexagonal ω, and (c) orthorhombic α'' phases. The differences in the vibrational free energies (diamonds) and in the electronic entropy contributions (crosses) to the free energy are also displayed.

in energy. Note that this is higher by about 550 K than the temperature at which the dynamical instability (softening of an optical mode) sets in. The temperature below which the β phase becomes dynamically unstable determines a lower limit to the martensitic start temperature.[10]

The same plot for the $\beta \rightarrow \omega$ transformation is shown in Fig. 14(b). In agreement with experiment we find the ω phase to be metastable only with respect to the α'' phase, and the $\beta \rightarrow \omega$ transition is predicted to occur only at a much lower temperature of about 200 K. Thus a thermal treatment above this temperature will lead to the formation of α'' precipitates, while the ω phase will be formed only upon aging at lower temperatures. These temperatures are lower than reported in the studies of Moffat and Larbalestier[3] and Kim *et al.*[10] Finally, the free-energy diagram for the $\beta \rightarrow \alpha'$ transition is shown in Fig. 14(a), displaying a calculated transition temperature of about 300 K.

Parts of the discrepancies between the calculated and observed transition temperatures could be due to the neglect of thermal expansion and of possible weak anharmonic effects in the phonon spectrum of the low-temperature phases, as well as to the approach used to optimize the chemical decorations of the different lattices. For the β phase the decoration has been optimized for a 16-atom supercell, while for the orthorhombic α'' phase only the different possibilities of locating the single Nb atom in a four-atom cell have been examined. It is hence conceivable that a slightly different chemical decoration of the orthorhombic α'' lattice reduces the structural energy difference and consequently, also the calculated transition temperature. Upon transformation from the β to the ω phase it has been assumed that the chemical decoration does not change at all.

Our models with the optimized chemical decoration also provide some rationale for the observed phase transformations: (i) The structures of the α'' and ω phases are derived by different deformations of the bcc lattice; hence no direct transformation between these phases will occur at low temperature. (ii) The $\beta \rightarrow \alpha''$ transformation involves a change of site occupation, while the $\beta \rightarrow \omega$ transformation does not. This explains why upon aging a slowly cooled sample below the martensitic temperature the metastable ω phase is formed, because during slow cooling the chemical order in the β phase is optimized. The lattice deformation producing the orthorhombic α'' phase is energetically unfavorable if applied to the G1 structure. In a quenched sample the more disordered distribution of the two species over the sites of the bcc lattice assumed at elevated temperatures is conserved, and this facilitates the formation of the α'' structure which requires a change in the site occupations relative to the optimal decoration of the bcc lattice of the β phase.

VI. CONCLUSIONS

We have constructed structural models for the β, α', α'', and ω phases of Ti_3Nb alloys with an optimized chemical decoration of the basic lattices. The static total energies from *ab initio* DFT calculations increase in the sequence $\alpha'' \rightarrow \omega \rightarrow \alpha' \rightarrow \beta$. While the structures of the low-temperature phases are found to be elastically and dynamically stable, the high-temperature β phase is found to be elastically stable but dynamically unstable below about 200 K, with imaginary frequencies for some optical modes. Using a self-consistent phonon approach we have shown that the soft phonon modes are stabilized already below room temperature. The temperatures for the $\beta \rightarrow \alpha''$ and $\beta \rightarrow \omega$ transitions have been calculated from the temperature dependence of the free energies, including the vibrational free energy and the electronic entropy contributions. In agreement with experiment, the lower transition temperature for the formation

of the ω phase shows that it can be formed only as a metastable phase.

We have shown that the chemical decoration of the basic lattices is essential for achieving elastic and dynamic stability of the β phase. While a $D0_3$-type superstructure of the bcc lattice (and many other possible chemical decorations) leads to an elastic instability and soft optical and acoustic modes which cannot be stabilized by anharmonic phonon-phonon interactions, the optimized G1 structure is stable against shear deformations and the soft optical modes are stabilized already at moderate temperature. The necessity to create an ordered distribution of the Ti and Nb atoms on the bcc lattice also has significant consequences for the phase transformations. Both the α'' and ω structures can be created by a continuous deformation of the bcc lattice. However, whereas the deformation of the G1 structure leads to a stable ω structure, the transition to the α'' structure also has to involve a change in the chemical decoration—which is possible at elevated temperature, but not in quenched samples. This provides a rationale for the observed competition between the formation of ω and α'' precipitates.

Our study has been motivated by the recent interest in gum-metal alloys, which differ from the binary Ti_3Nb alloy by the presence of small additions of other elements (Zr, Ta) and doping with a small amount of oxygen while maintaining the same electron/atom ratio. We think that the main conclusion of our work—the stabilization of the β phase by anharmonic phonon-phonon interactions—applies also to gum-metal alloys. However, the presence of ternary or quaternary additions might present a major obstacle to a change in site occupation and hence hinder the formation of a chemically optimized α'' phase.

Characteristic properties of gum-metal alloys include, besides their low shear moduli, their low ideal tensile and shear strengths. Current work is devoted to simulations of the response of β-phase Ti_3Nb alloys with the G1 structure to tensile and shear loading. Preliminary results show values of the ideal strengths close to experiment but very unusual stress-strain relations. More details will be reported very soon.

ACKNOWLEDGMENTS

We thank Dr. P. Souvatzis for making the SCAILD package available to us. Work at the Universität Wien was supported by the Austrian Science Fund (FWF) within the Special Research Program ViCoM (Vienna Computational Materials Laboratory, F41), through the VASP project, and in cooperation with the Toyota Central Research and Development Laboratory. The calculations were done at the facilities of the Vienna Scientific Cluster.

APPENDIX

The SCAILD method is based on the calculation of Hellmann-Feynman forces acting on atoms at locations displaced from their positions in an idealized lattice due to lattice vibrations (phonons). All phonons with wave vectors $\mathbf{q}$ commensurate with the supercell used for the calculations are excited and contribute to the displacements of the atoms from their equilibrium positions in a static lattice $\mathbf{R}+\mathbf{b}_j$ to new positions $\mathbf{R}+\mathbf{b}_j+\mathbf{U}_{\mathbf{R}j}$, where the displacements are given by

$$\mathbf{U}_{\mathbf{R}j}=\frac{1}{\sqrt{N}}\sum_{\mathbf{q}s}A^j_{\mathbf{q}s}\epsilon^j_{\mathbf{q}s}\exp^{i\mathbf{q}(\mathbf{R}+\mathbf{b}_j)}. \tag{A1}$$

Here $\mathbf{R}$ represents the N Bravais lattice sites of the supercell, $\mathbf{b}_j$ the position of atom j relative to its site, and $\epsilon^j_{\mathbf{q}s}$ are the phonon eigenvectors corresponding to the phonon mode $\mathbf{q}s$. The amplitudes $A^j_{\mathbf{q}s}$ of all phonon modes can be calculated in a harmonic approximation from the phonon frequencies $\omega_{\mathbf{q}s}$ as

$$A^j_{\mathbf{q}s}=\pm\sqrt{\frac{\hbar}{2M_j\omega_{\mathbf{q}s}}\coth\left(\frac{\hbar\omega_{\mathbf{q}s}}{2k_BT}\right)}, \tag{A2}$$

where T is the temperature of the system and M_j the mass of atom j. The phonon frequencies $\omega_{\mathbf{q}s}$ appearing in this expression can be obtained from the Fourier transform $\mathbf{F}^j_{\mathbf{q}}$ of the force constants acting on the atoms in the supercell by

$$\omega_{\mathbf{q}s}=\sqrt{-\sum_j\frac{\epsilon^j_{\mathbf{q}s}\mathbf{F}^j_{\mathbf{q}}}{A^j_{\mathbf{q}s}M_j}}. \tag{A3}$$

In the SCAILD scheme the equations are solved first by calculating a starting guess for the phonon dispersion relations by means of a standard supercell calculation using the direct-displacement method implemented in VASP.[65] The phonon frequencies corresponding to $\mathbf{q}$ vectors commensurate with the supercell are then used to calculate the atomic displacements using Eqs. (A1), (A2), and (A3). The forces induced by the displacements $\mathbf{U}_{\mathbf{R}j}$ are calculated using the VASP code. From the Fourier transform of the new force constants, a set of improved phonon frequencies is calculated using Eq. (A3). The mean value of the phonon frequencies calculated in all previous iterations provides a new set of frequencies:

$$\omega_{\mathbf{q}s}(N_i)=\frac{1}{\sqrt{N_i}}\sqrt{\sum_{i=1}^{N_i}\Omega^2_{\mathbf{q}s}(i)}, \tag{A4}$$

where $\Omega_{\mathbf{q}s}(i)$ are the frequencies from previous iterations. These steps are repeated until convergence is reached (hence the name "self-consistent phonon method"). In our calculations, about 100 iterations were necessary to obtain converged phonon frequencies, which makes SCAILD calculations considerably more expensive than usual direct-displacement or density-functional perturbation calculations of harmonic phonon frequencies. Anharmonicities associated with thermal expansion of the lattice are not included in the SCAILD scheme but might be taken into account by performing SCAILD calculations at several different volumes.

*juergen.hafner@univie.ac.at

[1] C. A. Luke, R. Taggart, and D. H. Polonis, Trans. ASM **57**, 142 (1964).

[2] E. W. Collings, *The Physical Metallurgy of Titanium Alloys* (American Society for Metals, Metals Park, OH, 1984).

[3] D. L. Moffat and D. C. Larbalestier, Metall. Trans. A **19**, 1677 (1988); **19**, 1687 (1988).

[4] C. Baker, Met. Sci. J. **5**, 92 (1971).

[5] S. K. Sikka, Y. K. Vohra, and R. Chidabaram, Prog. Mater. Sci. **27**, 245 (1982).

[6] S. Hanada and O. Izumi, Metall. Trans. A **17**, 1409 (1986).

[7] T. W. Duerig, J. Albrecht, D. Richter, and P. Fischer, Acta Metall. **30**, 2161 (1982).

[8] B. A. Hatt and V. R. Rivlin, J. Phys. D: Appl. Phys. **1**, 1145 (1968).

[9] H. Y. Kim, S. Hashimoto, J. I. Kim, H. Hosoda, and S. Miyazaki, Mater. Trans. **45**, 2443 (2004).

[10] H. Y. Kim, Y. Ikehara, J. I. Kim, H. Hosoda, and S. Miyazaki, Acta Mater. **54**, 2419 (2006).

[11] H. Hosoda, Y. Fukui, T. Inamura, K. Wakashima, S. Miyazaki, and K. Inoue, Mater. Sci. Forum **425-432**, 3121 (2003).

[12] H. Matsumoto, S. Watanabe, and S. Hanada, Mater. Trans. **46**, 1070 (2005).

[13] P. J. S. Buenconsejo, H. Y. Kim, and S. Miyazaki, Acta Mater. **57**, 2509 (2009).

[14] T. Grosdidier and M. J. Philippe, Mater. Sci. Eng. A **291**, 218 (2000).

[15] M. Tane, S. Akita, T. Nakano, K. Hagiharam, Y. Umakoshi, M. Niinomi, and H. Nakajima, Acta Mater. **56**, 2856 (2008).

[16] T. Saito, T. Furuta, J. H. Hwang, S. Kuramoto, K. Nishino, N. Suzuki, R. Chen, A. Yamada, K. Ito, Y. Seno, T. Nonaka, H. Ikehata, N. Nagasako, C. Iwamoto, Y. Ikuhara, and T. Sakuma, Science **300**, 464 (2003).

[17] H. Ikehata, N. Nagasako, T. Furuta, A. Fukumoto, K. Miwa, and T. Saito, Phys. Rev. B **70**, 174113 (2004).

[18] T. Furuta, S. Kuramoto, H. H. Hwang, K. Nishino, and T. Saito, Mater. Trans. **46**, 3001 (2005).

[19] S. Kuramoto, T. Furuta, J. H. Hwang, K. Nishino, and T. Saito, Metall. Mater. Trans. A **37**, 657 (2006).

[20] M. Y. Gudkin, T. Ishizaki, S. Kuramoto, and I. A. Ovidko, Acta Mater. **54**, 2489 (2006).

[21] S. Kuramoto, T. Furuta, J. Hwang, K. Nishino, and T. Saito, Mater. Sci. Eng. A **442**, 454 (2006).

[22] E. Withey, M. Jin, A. Minor, S. Kuramoto, D. C. Chrzan, and J. W. Morris, Mater. Sci. Eng. A **493**, 26 (2008).

[23] N. Takesue, N. Shimizu, T. Yano, M. Hara, and S. Kuramoto, J. Cryst. Growth **311**, 3319 (2009).

[24] J. W. Morris Jr., Y. Hanlumyang, M. Sherburne, E. Withey, D. C. Chrzan, S. Kuramoto, Y. Hayashi, and M. Hara, Acta Mater. **58**, 3271 (2010).

[25] E. A. Withey, A. M. Minor, D. C. Chrzan, J. W. Morris, and S. Kuramoto, Acta Mater. **58**, 2652 (2010).

[26] R. J. Talling, R. J. Dashwood, M. Jackson, S. Kuramoto, and D. Dye, Scr. Mater. **59**, 669 (2008).

[27] R. J. Talling, R. J. Dashwood, M. Jackson, and D. Dye, Scr. Mater. **60**, 1000 (2009).

[28] J. Sun, Q. Yao, H. Xing, and W. Y. Guo, J. Phys. Condens. Matter **19**, 486215 (2007).

[29] T. Li, J. W. Morris, N. Nagasako, S. Kuramoto, and D. C. Chrzan, Phys. Rev. Lett. **98**, 105503 (2007).

[30] C. Zener, in *Phase Stability in Metals and Alloys*, edited by P. S. Rudman, J. Stringer, and R. I. Jaffee (McGraw-Hill, New York, 1967), p. 25.

[31] G. Punz and J. Hafner, Z. Phys. B **65**, 465 (1987).

[32] E. G. Moroni, G. Grimvall, and T. Jarlborg, Phys. Rev. Lett. **76**, 2758 (1996).

[33] P. Souvatzis, O. Eriksson, M. I. Katsnelson, and S. P. Rudin, Phys. Rev. Lett. **100**, 095901 (2008).

[34] M. Born, Festschrift der Akad. d. Wissenschaften zu Göttingen, Math. Phys. Klasse (Berlin, Springer 1951).

[35] T. R. Koehler, Phys. Rev. Lett. **17**, 89 (1966); **18**, 654 (1967).

[36] Ph. F. Choquard, *The Anharmonic Crystal* (W. A. Benjamin, New York, 1967).

[37] W. Cochran and R. A. Cowley, *Handbuch der Physik* (Springer, Berlin, 1967).

[38] P. Souvatzis, D. Legut, O. Eriksson, and M. I. Katsnelson, Phys. Rev. B **81**, 092201 (2010).

[39] F. E. Wang, S. J. Pickart, and H. A. Alperin, J. Appl. Phys. **43**, 97 (1972).

[40] S. Prokoshkin, A. Korotitskyi, V. Brailovski, S. Turenne, I. Khmelevskaya, and I. Trubitsyna, Acta Mater. **52**, 4479 (2004).

[41] T. Waitz, D. Spišák, J. Hafner, and H. P. Karnthaler, Europhys. Lett. **71**, 98 (2005).

[42] X. Huang, G. Ackland, and K. Rabe, Nat. Mater. **2**, 307 (2003).

[43] M. X. Wagner and W. Windl, Acta Mater. **56**, 6232 (2008).

[44] N. Hatcher, O. Yu. Kontsevoi, and A. J. Freeman, Phys. Rev. B **80**, 144203 (2009).

[45] G. Kresse and J. Furthmüller, Comput. Mater. Sci. **6**, 15 (1996).

[46] G. Kresse and J. Furthmüller, Phys. Rev. B **54**, 11169 (1996).

[47] J. P. Perdew, J. A. Chevary, S. H. Vosko, K. A. Jackson, M. R. Pederson, D. J. Singh, and C. Fiolhais, Phys. Rev. B **46**, 6671 (1992).

[48] P. E. Blöchl, Phys. Rev. B **50**, 17953 (1994).

[49] G. Kresse and D. Joubert, Phys. Rev. B **59**, 1758 (1999).

[50] R. P. Feynman, Phys. Rev. **56**, 340 (1939).

[51] O. H. Nielsen and R. M. Martin, Phys. Rev. Lett. **50**, 697 (1983).

[52] T. Bučko, J. Hafner, and J. G. Ángyán, J. Chem. Phys. **122**, 124508 (2005).

[53] S. Müller, J. Phys. Condens. Matter **15**, R1429 (2003).

[54] Y. LePage and P. Saxe, Phys. Rev. B **63**, 174103 (2001).

[55] H. J. Monkhorst and J. D. Pack, Phys. Rev. B **13**, 5188 (1976).

[56] P. E. Blöchl, O. Jepsen, and O. K. Andersen, Phys. Rev. B **49**, 16223 (1994).

[57] M. Gajdoš, K. Hummer, G. Kresse, J. Furthmüller, and F. Bechstedt, Phys. Rev. B **73**, 045112 (2006).

[58] A. Togo, F. Oba, and I. Tanaka, Phys. Rev. B **78**, 134106 (2008).

[59] D. W. Taylor, Phys. Rev. **156**, 1017 (1967).

[60] S. de Gironcoli and S. Baroni, Phys. Rev. Lett. **69**, 1959 (1992).

[61] S. Ghosh, P. L. Leath, and M. H. Cohen, Phys. Rev. **66**, 214206 (2002).

[62] J. Hafner and G. Punz, Phys. Rev. B **30**, 7336 (1984).

[63] M. Fähnle and L. Schimmele, Z. Metallkd. **95**, 864 (2004).

[64] S. Dennler and J. Hafner, Phys. Rev. B **73**, 174303 (2006).

[65]G. Kresse, J. Furthmüller, and J. Hafner, Europhys. Lett. **32**, 729 (1995).
[66]D. Lerch, O. Wieckhorst, G. Hart, R. Forcade, and S. Müller, Modell. Simul. Mater. Sci. Eng. **17**, 055003 (2009).
[67]C. Blaas-Schenner, M. Stöhr, P. Lazar, R. Podloucky, J. Hafner, and R. Asahi (unpublished).
[68]D. Pattanayank, B. Obst, and U. Wolfsteig, Z. Metallkd. **72**, 481 (1981).
[69]K. S. Jepson, A. R. G. Brown, and J. A. Gray, *The Science, Technology and Applications of Titanium*, edited by R. I. Jaffee and N. E. Promisel (Pergamon Press, Oxford, 1970), p. 677.
[70]J. P. Morniroli and M. Gantois, memoires Scientifiques de la Revue de Metallurgie **70**, 831 (1973).
[71]M. Born and K. Huang, *Dynamical Theory of Crystal Lattices* (Clarendon Press, Oxford, 1954), p. 141.